

Article

Modeling the Spread and Control of COVID-19

Ashutosh Trivedi ¹, Nanda Kishore Sreenivas ² and Shrisha Rao ^{3,*}¹ Spext, Bengaluru 560053, India; ashu.trv@gmail.com² David R. Cheriton School of Computer Science, University of Waterloo, Waterloo, ON N2L 3G1, Canada; nandakishores1@acm.org³ International Institute of Information Technology Bangalore, Bengaluru 560100, India

* Correspondence: shrao@ieee.org

Abstract: Data-centric models of COVID-19 have been attempted, but have certain limitations. In this work, we propose an agent-based model of the epidemic in a confined space of agents representing humans. An extension to the SEIR model allows us to consider the difference between the appearance (black-box view) of the spread of disease and the real situation (glass-box view). Our model allows for simulations of lockdowns, social distancing, personal hygiene, quarantine, and hospitalization, with further considerations of different parameters, such as the extent to which hygiene and social distancing are observed in a population. Our results provide qualitative indications of the effects of various policies and parameters, for instance, that lockdowns by themselves are extremely unlikely to bring an end to an epidemic and may indeed make things worse, that social distancing is more important than personal hygiene, and that the growth of infection is significantly reduced for moderately high levels of social distancing and hygiene, even in the absence of herd immunity.

Keywords: COVID-19; SEIR; agent-based modeling; lockdown; hygiene; social distancing



Citation: Trivedi, A.; Sreenivas, N.K.; Rao, S. Modeling the Spread and Control of COVID-19. *Systems* **2021**, *9*, 53. <https://doi.org/10.3390/systems9030053>

Academic Editor: Oz Sahin

Received: 25 May 2021

Accepted: 28 June 2021

Published: 13 July 2021

Publisher's Note: MDPI stays neutral with regard to jurisdictional claims in published maps and institutional affiliations.



Copyright: © 2021 by the authors. Licensee MDPI, Basel, Switzerland. This article is an open access article distributed under the terms and conditions of the Creative Commons Attribution (CC BY) license (<https://creativecommons.org/licenses/by/4.0/>).

1. Introduction

The COVID-19 pandemic has presented humanity with grave social and economic challenges, and also a whole host of research questions that are not easily answered using standard statistical and other methods, in large part on account of the lack of sufficient data about the novel coronavirus SARS-CoV-2. Of particular interest is to understand emergent situations that may occur as a consequence of policy choices (e.g., lockdowns) and individual behaviors (e.g., observance of social distancing and personal hygiene). Policy-makers and the public at large can benefit by a better understanding of the macro-level consequences of the delicate micro-level behaviors of individuals. These macro-level consequences are emergent properties that arise from the interactions of a large number of diverse individuals who are part of the system.

Agent-based models (ABMs) help us consider such possible realities by creating and studying the effects of suitably designed agents in an interactive environment. Each agent represents an individual person with certain specific properties and behaviors. These agent properties are carefully chosen to model humans realistically, and agent behaviors are programmed keeping real behaviors in mind. With ABMs, it becomes feasible to study the complex system-level properties which arise from the interactions of individuals.

Certain specific aspects of our ABM for COVID-19 are a larger set of possible states that enable distinctions between asymptomatic and symptomatic infections, and parameters to model different levels of hygiene and social distancing. The model also allows for different levels of hospital care for differences in the severity of illness. Unlike statistical models, which often assume a homogeneous population, our model allows for agents with different levels of health, immunity, and comorbidity. Using simulations based on this ABM, we are able to evaluate different possible circumstances and observe their consequences.

The modeling of infectious disease outbreaks is a long-standing endeavor [1,2], but almost all efforts use mathematical (equation-based) modeling techniques [3]. There have also been specific efforts at modeling possible flu-like pandemics caused by H5N1 (“bird flu”) [4] and H1N1 (“swine flu”) [5].

In the case of the very real COVID-19 pandemic, there have also been numerous analytical efforts based on mathematical models [6,7], as well as data-driven models and projections [8,9].

Agent-based models have also been used in epidemiology [10–13], and to model specific instances, such as mosquito-borne diseases [14] and pandemic influenza [15]. Agent-based models have some advantages over mathematical models [16], such as in allowing for the consideration of heterogeneity in the population, discovery of emergent properties that are not readily apparent from the system description, and study of behaviors for which no closed-form mathematical description is easily available.

There are also some early efforts at modeling COVID-19 using agent-based models [17,18].

The present work is distinct in that we create an extended agent-based model that allows for qualitative evaluations of the effects of social distancing, personal hygiene, and lockdowns, while taking into account the epidemiological characteristics of COVID-19 [19] and the heterogeneity of populations of people who may become affected. The basic SEIR model and its common extensions are not entirely adequate to model the spread of the disease, as they do not take into account the classification of infectious states by types— asymptomatic, symptomatic (but not hospitalized), hospitalized, and needing intensive care—which is a concern in reality [20].

In our model, each agent represents a human in society who interacts with others. Human movements and interactions are captured by motion and occasional proximity in a two-dimensional grid. Each agent has certain characteristics (see Section 3.2.1 for details), and some agents change states based on infections and recovery. Our model allows us to understand the difference between a black-box view of the epidemic and a glass-box view (Section 3.1). It also allows us to control agent parameters in accordance with the characteristics of different people in a large human population (Section 3.2), and to change the characteristics of the system to model the effects of different policies and public-health practices (Section 3.2.2).

Our model, as with any ABM, does not guarantee quantitatively precise results, but the findings are qualitatively meaningful, in the sense that they correctly indicate the effects of various agent parameters and behaviors, and system control measures.

Our results are in line with expectations; e.g., it is suggested by Schueller et al. [21] that lockdowns slow down the spread of COVID-19 and reduce the peak of infections. Silva et al. [18] propose an agent-based model that allows the simulation of social distancing and the use of masks (as a specific measure of personal hygiene), and study their effects in certain scenarios, with similar but incomplete results.

The following are some of the findings of our work:

1. Social distancing is more important than personal hygiene (Section 4.3).
2. Social distancing and hygiene together are more important than lockdowns for controlling the spread of disease (Section 4.4). In fact, in their absence, a lockdown can do more harm than good; without social distancing and hygiene, a post-lockdown peak of cases can be higher than without the lockdown, with a similar effect also observed with more stringent lockdowns as compared to more relaxed ones (Figure 7).
3. When the fraction of the population that is immune to the disease (either by vaccination or by previous exposure or recovery) is small, e.g., 20%, the peak of infectious cases can be nearly as high, in the absence of social distancing and personal hygiene, as when there is no immunity at all in the population (Section 4.5). Even in the case in which approximately 40% of the population is immune, there can be a large number of infections in the absence of social distancing and hygiene (Figure 12b).
4. Proper herd immunity in the classical sense is said to occur (in the total absence of social distancing and hygiene) only when a large fraction of the population becomes immune [22]. However, when the smaller fraction of 40% of the population is immune

(i.e., the fractional immunity of the population is 0.4), this can be achieved with some observance of social distancing and hygiene; the same effect is also possible with an even smaller fraction of 20% of the population being immune, with a rigorous observance of social distancing and hygiene (Section 4.5).

5. Surges in hospital capacity (including critical care capacity) help reduce the number of severely ill people dying due to a lack of access to medical care, but do not directly affect the overall number of cases to a significant extent (Section 4.6).

2. Disease Model

A common way of modeling the spread of infectious diseases is using the SIR (susceptible–infectious–recovered) model [1], which is a *compartmental* model that divides the entire population into three classes. The *susceptible* state consists of individuals who may become infected; the *infectious* individuals are those currently afflicted with the disease; and *recovered* individuals are ones who have overcome the disease.

An extension of this is the SEIR model [1] that also allows for an *exposed* state where an individual has received a load of the pathogen, but is not yet infectious or symptomatic. In the SEIR model, it is generally assumed that recovered individuals have lifelong immunity.

Both the SIR and SEIR models are generally based on differential equations, and allow for various types of qualitative analyses [23,24].

We modify the usual SEIR model to also include multiple infectious states, and to show when someone is deceased.

2.1. Modified SEIR

The primary motivation for this modification is the observation that in COVID-19 (but also in other diseases), the infectious state is not truly a single state describing all infected individuals. Rather, there are multiple types of infectious states:

- I_0 This is the *infectious asymptomatic* state, where an individual does not show signs of the disease at all, but can transmit it to others. It is presently believed that a large number of infected people recover directly from this state, and that coming into proximity with such asymptomatic individuals is responsible for a large fraction of the COVID-19 spread [25].
- I_1 This is the *infectious symptomatic* state, where an individual shows signs of the disease, but is not (yet) hospitalized, either because the symptoms are considered mild enough, or because hospital care is unavailable.
- I_2 This is the *infectious hospitalized* state, where an individual shows signs of the disease and receives hospital care.
- I_3 This is the *infectious critical care* state, where the individual is severely afflicted and receives critical care in an ICU or similar unit, including with specialized devices, such as ventilators.

In addition to this, we add a distinguished state D to the model, showing when a sick individual is deceased as a consequence of the illness. The modified SEIR model is shown in Figure 1.

This model is slightly similar to the one proposed by Arino et al. [6], which also considers multiple types of infectious states, but this model is based on differential equations and thus not directly applicable in an ABM context.

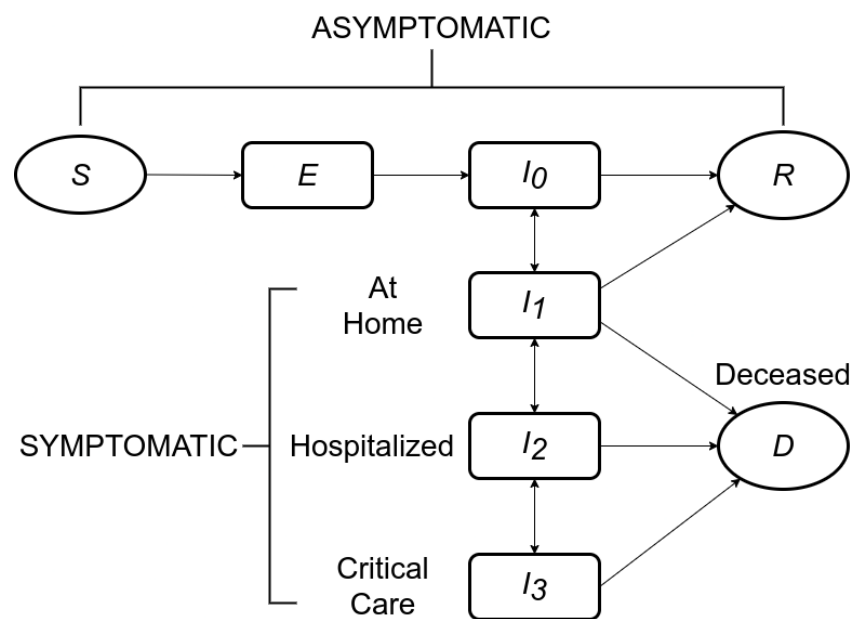


Figure 1. Modified SEIR model for COVID-19, with multiple infectious states.

2.2. State Transitions

The state transitions between different states for an individual are also as indicated in Figure 1. These are as follows.

$S \rightarrow E$ The state transition from *susceptible* to *exposed* happens when a susceptible individual comes into close contact with an infectious individual (someone in any of the states I_0 , I_1 , I_2 , or I_3). Each infectious individual has an infection range, and if another individual comes within their infection range, they are said to be in close contact. The state transition from S to E is considered instantaneous (see Section 3.3.1).

$E \rightarrow I_0$ The state transition from *exposed* to *infectious asymptomatic* happens upon the completion of the *latent period* of the disease, starting from the instant of exposure (see Section 3.3.2).

$I_0 \rightarrow I_1$ The state transition from *infectious asymptomatic* to *symptomatic* happens upon the completion of the *incubation period* of the disease, starting from the instant of exposure. In many individuals, this transition may not happen at all, and the individual may instead transition to R (*recovered*) directly (see Section 3.3.2).

$I_1 \rightarrow I_2$ The state transition from *infectious symptomatic* to *hospitalized* happens in some infected individuals when the symptoms worsen to the point of requiring hospital care (see Section 3.3.3).

$I_2 \rightarrow I_3$ The state transition from *hospitalized* to *critical care* happens in some individuals whose aggravated conditions require ICU and similar critical care (see Section 3.3.4).

$I_* \rightarrow D$ The state transitions from I_1 , I_2 , and I_3 to D (*deceased*) happen in some individuals. Individuals who are in I_1 and I_2 and in need of more advanced care (in I_2 and I_3 , respectively) are at increased risk of transition to D when such care is unavailable. Individuals in I_3 are at increased risk of transitioning to D with increasing time spent in that state (see Section 3.3.5).

3. Agent Model

In this section, we describe our agent model and its workings. In Section 3.1, we first encapsulate the difference between black-box and glass-box views of the spread of COVID-19, which is highly important for understanding why this pandemic has proven so difficult to tackle. Section 3.2 describes the primary characteristics of the agents as well as the system in which they are placed. Section 3.3 describes the state transitions of agents.

3.1. Black-Box and Glass-Box Views

In terms of modeling the occurrence of COVID-19 or any similar disease in a population, we find it useful to incorporate the distinction between black-box and glass-box views of the epidemic.

The black-box view of the epidemic corresponds to the observation of the incidence and spread of the disease in an affected population without widespread testing and tracing—agents only become ill with disease symptoms, and some need to be hospitalized, while others apparently stay healthy. Except in the case of symptomatic cases, it is not known who may carry the infection. This is related to, but not the same as, the standard definition of *black box epidemiology*: “the use of observational epidemiological methods and inference to arrive at conclusions about cause-effect relations between risk factors and disease” [26].

The glass-box view of the epidemic is the idealized condition where there is perfect knowledge of the extent of the epidemic, both in terms of the agents that are infected, and the exact state that each agent is in. This too is not the same as the standard *white box epidemiology*, such as that seen in the putative correlation between night-shift work and an increased risk of cancer [27].

As may be expected, in general, far fewer agents are known to be infected in the black-box view, as asymptomatic infections are unseen. This leads to the situation depicted in Figure 2, where Figure 2a shows the black-box view, the limited perspective with relatively few agents showing symptoms, and Figure 2b shows the glass-box view, the real situation with many infected and exposed agents in the population.

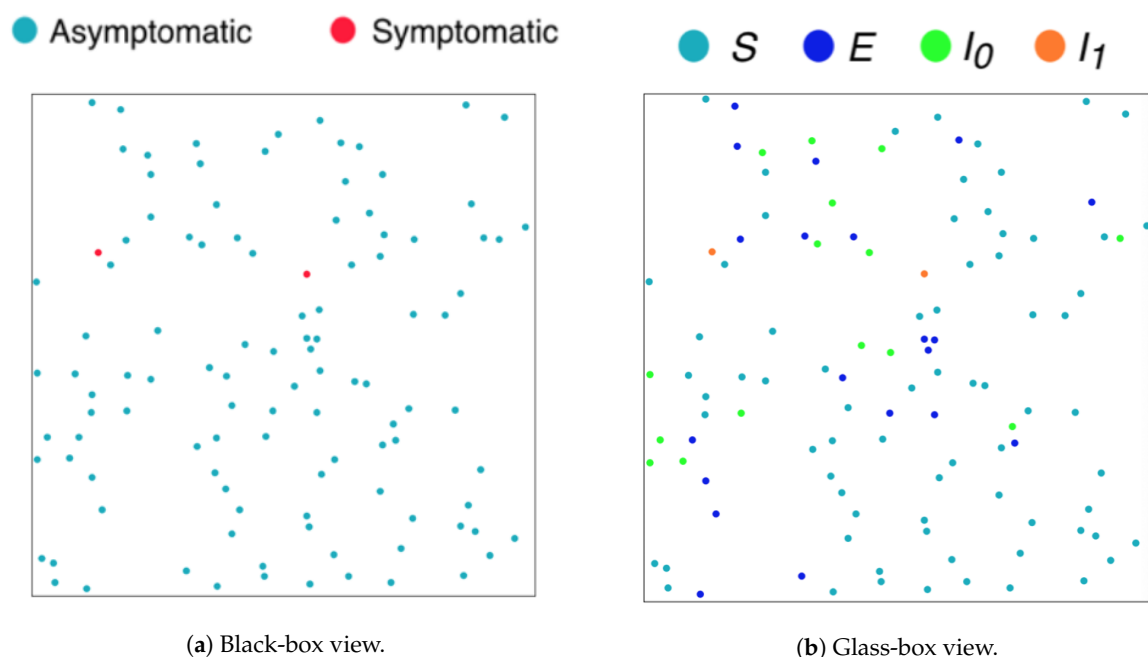


Figure 2. Two views of an epidemic at an early stage.

Another aspect of the difference between the black-box and glass-box views may be seen from Figure 3, which shows the apparent progress of the epidemic over time. The higher line corresponds to the glass-box view, where a much larger fraction of the population is seen to contract the infection. The lower line corresponds to the black-box view, where a much smaller fraction of the population develops symptoms and is known to be infected.

The distinction between the black-box and glass-box views is made possible by the extended SEIR model depicted in Figure 1, which shows that the states S , E , I_0 , and R are all asymptomatic, and thus agents in these states appear not to be infected. An agent that is in state I_0 is counted as infected in the glass-box view, but not in the black-box view. Agents

that undergo the transition $S \rightarrow E \rightarrow I_0 \rightarrow R$, i.e., are exposed, infected, and subsequently recover without showing symptoms, and are not known to have been infected at all.

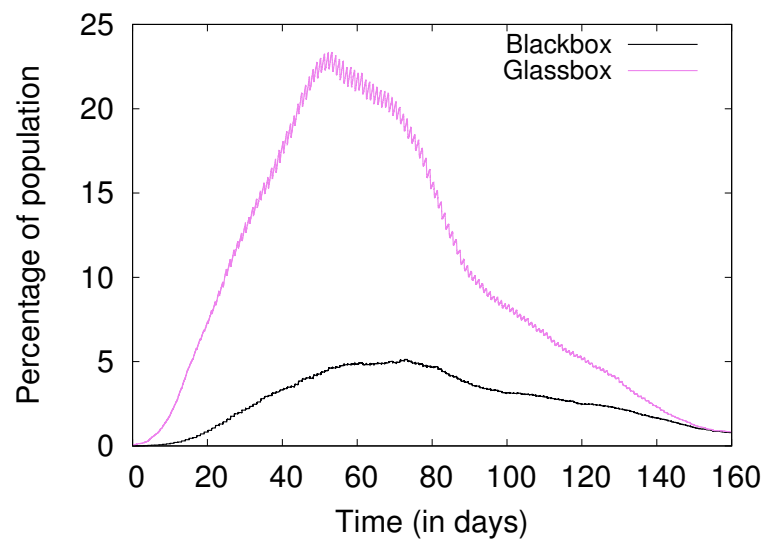


Figure 3. The progress of an epidemic, glass-box vs. black-box views.

3.2. Individual and Social Attributes

We model humans in a society as a collection of agents, where each agent is a computational structure that captures some essential aspects of humans that are relevant to disease progression and spread. Some attributes are at an agent level, such as age and health, while others are at a social level, such as lockdown efficacy and social distancing. We discuss the agent characteristics in Section 3.2.1 and the system parameters in Section 3.2.2.

One of the specific metrics that is often in connection with the COVID pandemic and other outbreaks is R_0 , the “basic reproductive ratio”. This is a number greater than or equal to 0, and is supposed to show how many others are infected, on average, by a single infected individual [28]. A value of R_0 below 1 shows that the case is declining, while a value greater than 1 suggests that each infected person infects more than one other person on average, so that the case count increases with time. However, the R_0 metric is very complex [29] and can be quite misleading if not entirely meaningless [30]. As such, given that our work deals with fine-grained modeling rather than the measurement or estimation of coarse statistical outcomes, we chose not to measure the values of R_0 generated in our models.

3.2.1. Agent Characteristics

An agent Y is formally defined as a five-tuple as follows:

$$Y = \{a, \beta, h, c, \omega\}$$

The agent attributes are:

- a is the age, $0 < a < 90$.
- β denotes the level of hygiene, $0 \leq \beta \leq 1$.
- h denotes the level of overall health, $h \in \{0, 1, 2, 3\}$.
- c denotes comorbidity level, $c \in \{-2, -1, 0\}$.
- ω denotes the immunity, $\omega \in \{0, 1\}$.

These five attributes are further used to calculate the recovery score (r) and age score ($f(a)$), which are described in the following paragraphs, and are given by (1) and (2).

Age has been shown to be highly relevant to disease progression, with the elderly most at risk for worse outcomes [31].

The attribute β is included to model hygiene as seen in the real world in the form of protective masks, sanitizers, PPE, etc. This is particularly relevant in the inter-personal

transmission of the virus, which is described in detail in Section 3.3.1. A value of 1 corresponds to perfect hygiene, and 0 corresponds to a complete lack of hygiene, with higher levels of hygiene correlated with lower chances of transmission.

We model health (h) as a 4-step discrete parameter from 0 to 3. A value of 3 denotes an agent in perfect health, and a value of 0 denotes an agent in poor health.

It is known that people with comorbid conditions have a higher death rate, and the death rate further varies based on the comorbid condition itself, with some conditions being worse than others [32]. A comorbidity (c) value of 0 implies the agent has no comorbid conditions, and a value of -2 implies the agent has the worst comorbid condition.

Immunity plays a major role in determining the speed of disease progression [33]. Weak immune response enables the virus to multiply quickly and quickens the onset of symptoms and infectiousness. In our model, immunity can take a value of either 0 or 1, with 0 corresponding to an immunosuppressed agent, and 1 corresponding to an agent with strong immune response.

We introduce recovery score (r) as an integrated metric that aggregates all these agent attributes, and directly correlates to the chances of recovery of an infected agent. Unlike all the other attributes, age has a very long range and, therefore, becomes difficult to combine with other attributes. Hence, age has to be transformed to a similarly small range as the other attributes.

The effect of age on susceptibility to infection is quite complex [34,35]. However, in the case of COVID-19, it is known that younger segments of the population (those below middle age) are generally less susceptible to infection, and that such susceptibility increases in middle age and becomes quite large for the elderly [31]. Based on this, we propose a function (f) mapping the age of an agent with the infection risk, as follows:

$$f(a) = \begin{cases} 0 & a > 60 \\ 1 & 0 < a < 40 \\ 2 & 40 \leq a \leq 60 \\ 3 & 1 \leq a < 40 \end{cases} \quad (1)$$

The age score function $f(a)$ maps age, a , to a range of 0 to 3, where lower values correspond to higher risks. Using this age score in place of the actual age, we are able to obtain all the attributes in a similar range and direction, i.e., higher values of all attributes are positive, and lower values correspond to a higher risk of worse outcomes.

The values of these agent attributes are now added together to obtain an integrated recovery score (r), which is a measure of the agent's chances of recovery, and is given by:

$$r = f(a) + h + c + 2 \quad (2)$$

It is offset by 2 to counter the negative values of comorbidity and ensure the metric remains in the positive range. Hence, it can be seen that $0 \leq r \leq 8$.

3.2.2. System Parameters

In our model, we have five system-level parameters as follows:

- α denotes the efficacy of social distancing, $0 \leq \alpha \leq 1$.
- κ denotes the lockdown efficacy, $0 \leq \kappa \leq 1$.
- L denotes the lockdown duration, in days, $L > 0$.
- b denotes the number of beds per 1000 agents, $b > 0$.
- Π denotes the fractional immunity in the system, $0 \leq \Pi \leq 1$.

Social distancing has been widely used as a policy to slow the spread of disease in many places. There are many interactions between agents in a simulation, and social distancing is said to be followed in such an interaction if the agents are outside the infection ranges of each other. If social distancing is followed in a particular interaction, then there is no disease transmission due to the abovementioned interaction. We define social distancing

efficacy (α) as the ratio of the number of interactions where social distancing was followed to the total number of interactions.

Lockdown has been used as a strategy to various degrees by various countries to “break the chain” and slow the spread of infection. In a complete lockdown, all agents are static, and their movements are completely restricted. However, more generally, not all agents observe lockdown, and some continue to move around, and this is modeled through a lockdown efficacy parameter (κ). Another parameter of a lockdown is the duration, denoted by L . For example, a lockdown with $L = 30$ and $\kappa = 0.8$ implies there is a 30 day lockdown with 20% of agents still mobile, but the other 80% of agents are completely static.

To consider cases where a fraction of the population is immune to the disease, either from previous exposure and recovery, or by immunization or natural immunity, we define a parameter called *fractional immunity*, denoted as Π , which shows the fraction of the agent population that is immune at the outset of a simulation. This notion of fractional immunity is similar to that seen in studies that seek to model the effect of a pre-existing or acquired immunity already present in a significant fraction of the population [36,37].

Hospitals are considered to have two types of resources—normal beds and ICU beds. The normal beds are for agents in I_2 , and the ICU beds are for those in the more critical I_3 . The bed capacity of the system, denoted by b , is the number of beds per 1000 agents in the system.

3.3. State Transitions

The state transitions are as defined in Section 2.2, and their transition probabilities are described here. The probability of state transition from S to E is computed once for every interaction with an infectious agent, as described in Section 3.3.1. However, the rest of the transition probabilities, given by (4)–(13), are all computed on a daily basis, and if none of the possible transitions occur on any given day, then the agent continues in the same state.

3.3.1. Transition from S , the Susceptible State

Conventional methods of estimating disease transmission probability use differential equations and such tools, and work with populations rather than considering individual interactions [38,39]. However, in an agent-based model, the probability of transmission cannot be constant and uniform across all interactions, and should be based on the interacting agents’ attributes.

A susceptible agent A in state S can become exposed to the virus through an interaction with another infectious agent B . If social distancing is followed in this interaction, then agent A is not exposed, and continues to remain in S state even after the interaction. However, if social distancing is not practiced, then the chances of transmission depend on the levels of hygiene (β) of both agents. The levels of hygiene of A and B may be denoted by β_A and β_B , respectively. The probability of infection, denoted by $p(A, B)$ is given by:

$$p(A, B) = \rho(1 - \beta_A)(1 - \beta_B) \quad (3)$$

where $0 < \rho \leq 1$ is a scaling constant. If either agent practices perfect hygiene, transmission would not occur, and this holds in our model as well by Equation (3). Otherwise, the agent A now transitions from S to E with a probability of $p(A, B)$ due to the said interaction.

3.3.2. Transitions from E , the Exposed State, and I_0 , the Asymptomatic State

The duration between an agent first reaching states E and I_1 is termed as the *incubation period* (λ). The *latent period* (Φ) refers to the duration between states E and I_0 . In the case of COVID-19, the latent period is known to be smaller than or equal to the incubation period [40]. Accordingly, the latent period is fixed such that $1 \leq \Phi \leq \lambda$.

The incubation period depends on a number of factors, including host immunity (ω) and age (a) [33,41]. The minimum, maximum and average values are denoted by λ_{min} , λ_{max} , and $\bar{\lambda}$, respectively. Current studies on COVID-19 indicate that the incubation period is between 2 and 14 days [42] with a mean of 5 days [43].

To calculate the transition probability for a weak immune agent with $\omega = 0$, we use the following expressions. We sample a number x from a uniform distribution between 0 and 1. The agent transitions to I_1 directly from E if the below condition is met:

$$\frac{1}{\bar{\lambda}} \leq x \leq \frac{1}{1 + f(a)} \quad (4)$$

This creates a higher probability of transition to the I_1 state if the age score $f(a)$ is lower, since the range in which x is allowed to fall now has a larger window based on the age score.

If an agent has strong immunity ($\omega = 1$), it has a lower chance of directly transitioning into the state I_1 , as given by the following:

$$0 \leq x \leq \frac{1}{k_1 \times \lambda_{max}} \quad (5)$$

If the agent is in the E state, there is a chance of moving to state I_0 . For both weak and high immune agents, we use the following expression. We sample another number y from the same uniform distribution, and calculate the transition for I_0 by:

$$\frac{1}{\bar{\lambda} - 2} \leq y \leq \frac{1}{\bar{\lambda} - 3} \quad (6)$$

Sakurai et al. [44] indicate that the duration to the resolution of infection for asymptomatic individuals is in the range of 3 to 21, and indicate that a considerable portion of asymptomatic individuals recover within 15 days. In our model, if an agent in I_0 does not transition to I_1 within 12 days, then it is considered recovered and moves to R .

3.3.3. Transitions from I_1 , the Symptomatic State

A symptomatic infectious agent in I_1 can transition to I_2 , D , or R , as seen in Figure 1. Multiple factors, such as the recovery score (r) given by Equation (2), the number of days spent in I_1 (d_{I_1}), and the availability of hospital care, determine the next transition. If hospital beds are available, the agent transitions from I_1 to I_2 with a probability given by:

$$p(I_1, I_2) = 1 - \frac{r - (k_2 \times d_{I_1}) + 2}{10} \quad (7)$$

The probability of transition from I_1 to I_2 depends on the recovery score (r) and time spent in state I_1 (d_{I_1}). If r is high, it is less likely for the agent to move to state I_2 . If an agent spends more time in I_1 , then the probability of transitioning to I_2 is greater. Therefore, we use both parameters to calculate the probability $p(I_1, I_2)$. We use a multiplicative constant k_2 to rescale d_{I_1} to be in the same range as r . As this is a probability, and hence should be between 0 and 1, the expression is scaled and offset appropriately.

However, if a hospital bed is not available, then the agent probabilistically transitions to death, D , as given by:

$$p(I_1, D) = k_3 \times p(I_1, I_2) \quad (8)$$

Additionally, if the agent remains in I_1 for more than 12 days, then it recovers and transitions to R . This is with a small margin over the 10 days of infectivity indicated by the CDC [45].

3.3.4. Transitions from I_2 , the Hospitalized State

An agent in I_2 can transition to I_3 , I_1 , or D . These transitions also depend on the recovery score (r), duration in I_2 (d_{I_2}), and the availability of ICU if needed. If ICU care is available, then the agent transitions from I_2 to I_3 with a daily probability given by:

$$p(I_2, I_3) = 1 - \frac{r - (k_2 \times d_{I_2}) + 2}{10} \quad (9)$$

This equation is very similar to (7), and the scaling is carried out similarly as well. If ICU care is not available, then the agent transitions to D with a probability given by:

$$p(I_2, D) = k_3 \times p(I_2, I_3) \quad (10)$$

The daily probability that the agent transitions to I_1 and becomes better is given by:

$$p(I_2, I_1) = \frac{r}{8 \times d_{I_2}} \quad (11)$$

“Prolonged Length-of-stay (PLOS) [in hospital] is associated with increased mortality and other poor outcomes” [46]. In line with this, the probability of an agent in I_2 reverting to I_1 should be inversely proportional to the hospitalized duration (d_{I_2}), as seen in (11).

3.3.5. Transitions from I_3 , the Critical State

An agent in I_3 can either transition to D or I_2 , and this depends on the recovery score (r) and the duration in ICU (d_{I_3}).

The agent transitions to death with an increased probability as the time spent in ICU increases; a lower value of recovery score also implies a higher risk of death. Therefore, the daily probability of dying is given by:

$$p(I_3, D) = 1 - \frac{r - (k_2 \times d_{I_3}) + 2}{10} \quad (12)$$

This is similar to the worse transitions from I_1 and I_2 , and the same scaling factors are used here as well.

The daily probability of progressing and moving back to I_2 is given by:

$$p(I_3, I_2) = \frac{r}{8 \times d_{I_3}} \quad (13)$$

Agents with a higher recovery score have better chances of recovering, and hence $p(I_3, I_2)$ is proportional to r , as seen in (13).

4. Experiments and Results

In this section, we discuss the experiments we performed with agents and the disease model we described previously.

4.1. Simulation Environment

Our simulation experiments were performed by circular agents in a 2-D enclosed planar environment. The environment scales based on the number of agents. We performed all our simulations with 20,000 agents. Our simulations ran for 160 simulated days, where 500 simulation cycles correspond to 1 simulated day, and thus makes for a total of 80,000 cycles for one experiment.

The initial range of values of each agent attribute is presented in Table 1. It is of course not possible to claim that these (or any other) simulation settings precisely describe all real scenarios, but wherever possible, we calibrated the model to be close enough to real parameters according to prior sources [31–33,47].

For every experiment, a population of agents was initiated and unique properties were assigned based on the range and distributions described in Table 1. Most agents were in the susceptible state (S) initially, but a small fraction of agents were in I_0 and began propagating the disease (see Section 4.2).

Each agent has attributes as described in Section 3.2.1, and the age score and recovery score were calculated using Equations (1) and (2), respectively.

In each simulation cycle, every agent was triggered and followed Brownian motion (as used to model human crowd movement [48,49]) and updated its location in the environment. Each agent has an identical infection range around it. Due to random motion, if

any susceptible agent comes within this range of an infectious agent, there is a chance that infection can be transferred to the susceptible agent. This chance depends upon the level of personal hygiene β for both agents, as calculated by Equation (3). Similarly at every trigger, each agent's state transition probabilities were calculated and updated as described in Section 3.3.

Table 1. The presence of a dash indicates that there is no pre-set range for that parameter.

Variable	Symbol	Range
Hygiene	β	[0, 1]
Hygiene population mean	$\bar{\beta}$	[0, 1]
Age	a	[0, 90]
Health	h	{0, 1, 2, 3}
Comorbidity	c	{−2, −1, 0}
Immunity	ω	{0, 1}
Social distancing	α	[0, 1]
Fractional immunity	Π	[0, 1]
Lockdown efficacy	κ	[0, 1]
Transmission constant	ρ	0.25
Incubation period	λ	[1, 14]
Latent period	Φ	[1, 14]
Recovery score	r	{0, 1, 2, ..., 8}
Bed capacity	b	$0 \leq b \leq 1000$
Duration in I_*	d_{I_*}	—
Scaling constants	k_*	—

Given some policies applied in a given day, some of the agent behaviors are controlled by said policies. For example, during a lockdown, the location of the agents is not updated; when social distancing is observed, an agent's location is not permitted to be within the infection range of other agents.

To simulate isolation during quarantine, we removed agents from the environment and kept them in a different quarantine environment for 14 days. Once they were recovered or upon completion of this duration, they were again sent back to the main environment. Deceased agents were removed from the environment completely. All our simulations not only produce output data, but can also be visualized as seen in Figure 2a,b.

We used the MASON [50] simulation library, a Java simulation toolkit that scales well with a large number of agents and also helps in generating visuals of environment and agents. We used AWS C3 (compute optimised) Linux VMs with 4-core CPU and 8 GB RAM.

4.2. The Base Case

This corresponds to the unrestricted spread of a contagion through an enclosed, initially completely susceptible population. Even in this case, symptomatic infected (I_2, I_3) agents are isolated from the rest of the population. The number of isolated agents depends on hospital bed and ICU bed availability. Otherwise, everything proceeds as usual, with no restrictions on movement, no social distancing and no lockdowns.

One way to instantiate the base case is to admit a fixed number of infected agents into the population. The agents' ages were sampled from a triangular distribution with a peak of 25, and a range of 0 to 90. The mean hygiene level of the population is 0.6. At random, 3% of the population was assigned weak immunity in line with a study conducted in the US [51]. To start the onset of infection, we started with 0.005% of infected agents already in the system. The incubation period was kept to a maximum of 14 days.

In the baseline as well as in other cases, the default hospital bed availability is 2 beds/1000 population [47]. We assume the availability of 1 ICU bed per 20 hospital beds.

Figure 4 shows the percentage of agents in each infectious state versus time, for the base case. We can see that the peak of asymptomatic (I_0) cases is reached just before day 60. Similar peaks are seen for I_1, I_2 , and I_3 cases but with a delay, as observed in reality.

The load on the public health infrastructure and the peak demand of critical care can be understood from the I_2 and I_3 curves. On day 120, the demand for hospitalization peaks, and roughly 1% of the entire population requires hospitalization at this stage.

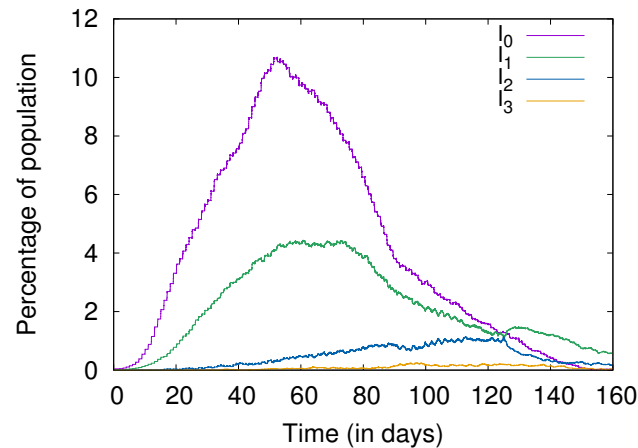


Figure 4. Baseline.

Figure 5 also shows the cumulative numbers of infected, recovered, and deceased for the base case. Without any social distancing or other measures, the disease spreads fast, nearly every agent in the population is eventually infected, and most subsequently recover by day 160. It can also be seen that only about 30% of the agents show symptoms, even though the entire population was infected at one time or another. This shows that most agents (70%) progress to the I_0 (asymptomatic) state but no further, as seen in reality as well [52].

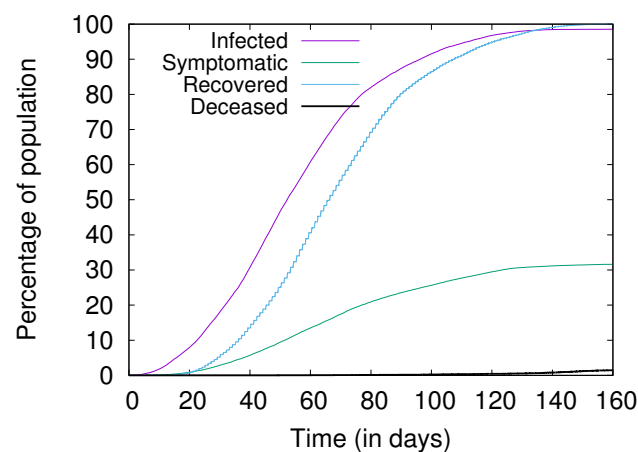


Figure 5. Cumulative figures of infection, recovery, and death.

4.3. Hygiene and Social Distancing

It has been repeatedly stated that maintaining personal hygiene and social distancing are the key to slowing down the spread of COVID-19. In this experiment, we compared the effects of two strategies—(i) a high value of average personal hygiene with moderate social distancing ($\beta = 0.9, \alpha = 0.7$), and (ii) a high average social distancing with moderate personal hygiene ($\beta = 0.7, \alpha = 0.9$).

Through simulation, we found that social distancing is more important than personal hygiene. As seen in Figure 6, the higher social distancing scenario reduces the peak load by about 50% when compared to the higher personal hygiene scenario. However, it is seen that both these cases are much better than the baseline.

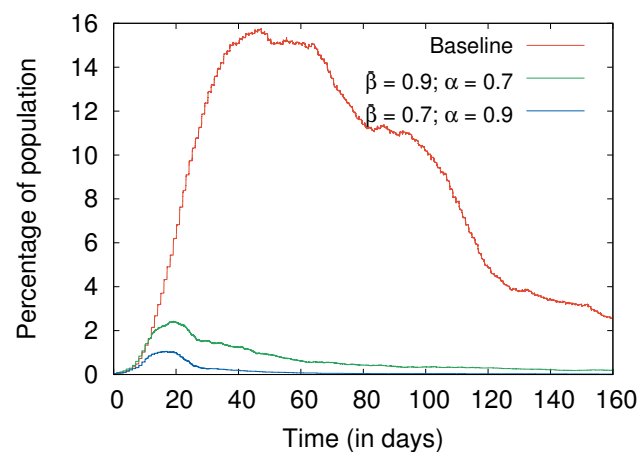


Figure 6. Comparing high hygiene and high social distancing.

Varying both the mean personal hygiene and social distancing efficacy in the range of 0.4 to 0.9, we ran 10 simulations for each pair to understand the peak values and when they occurred. The average peak values and the median of days on which these peaks occur are shown in Table 2. With the increasing mean hygiene $\bar{\beta}$, the peak days are delayed for all infectious states. It can be seen that increasing both $\bar{\beta}$ and α reduces the number of deaths, as expected. However, there is a bigger reduction in the number of deaths for every 0.1 increase in α as compared to the same 0.1 increase in $\bar{\beta}$. A similar trend is also seen in the peak values. The number of deaths is negligible for high values of α , such as 0.8 and 0.9, even with lower values of $\bar{\beta}$, but similar high values of $\bar{\beta}$ with lower α do not reduce the deaths to the same extent. Once again, this shows that social distancing is more important than personal hygiene.

Table 2. Peak values and deaths for different values of hygiene and social distancing.

β	α	Peak Values (%)			Median Peak Day			D (%)
		I_1	I_2	I_3	I_1	I_2	I_3	
0.40	0.40	3.12	0.97	0.24	76	148	138	0.53
0.40	0.60	1.73	0.60	0.12	119	157	152	0.18
0.40	0.80	0.02	0.01	0.01	25	43	27	0.00
0.40	0.90	0.01	0.00	0.00	14	–	–	0.00
0.60	0.40	2.60	0.88	0.21	83	157	146	0.46
0.60	0.60	1.14	0.41	0.10	135	158	148	0.13
0.60	0.80	0.02	0.01	0.00	20	18	–	0.00
0.60	0.90	0.01	0.00	0.00	14	–	–	0.00
0.80	0.40	2.33	0.76	0.17	107	158	149	0.29
0.80	0.60	0.56	0.18	0.05	158	155	152	0.06
0.80	0.80	0.01	0.00	0.00	16	3	–	0.00
0.80	0.90	0.01	0.00	0.00	10	4	–	0.00
0.90	0.40	2.39	0.76	0.15	118	158	149	0.25
0.90	0.60	0.51	0.16	0.04	153	152	154	0.04
0.90	0.80	0.02	0.00	0.00	13	6	–	0.00
0.90	0.90	0.01	0.00	0.00	11	3	–	0.00

4.4. Lockdowns

Lockdown is another strategy that has been used in some form across many countries to combat the spread of COVID-19. In a set of experiments to study its effects, when lockdown is applied, agents are immobile. In practical settings, perfect lockdowns are impossible (due to some people being essential workers, or defiant of the lockdown policy), so we simulated partial lockdowns using a parameter of lockdown efficacy (κ), which

is the fraction of agents who follow the guidelines fully and stay completely immobile during this period. However, even immobile agents can always come into contact with other agents who are mobile and not observing the lockdown policy. We experimented with different values of κ to observe its effects on the infection spread.

We ran experiments of imposing a 30-day lockdown, starting on day 10, with varying efficacy. In Figure 7, we can see that during a 30-day lockdown period, the infection rises faster with $\kappa = 0.7$ compared to tighter and strict lockdown with efficacy 0.9.

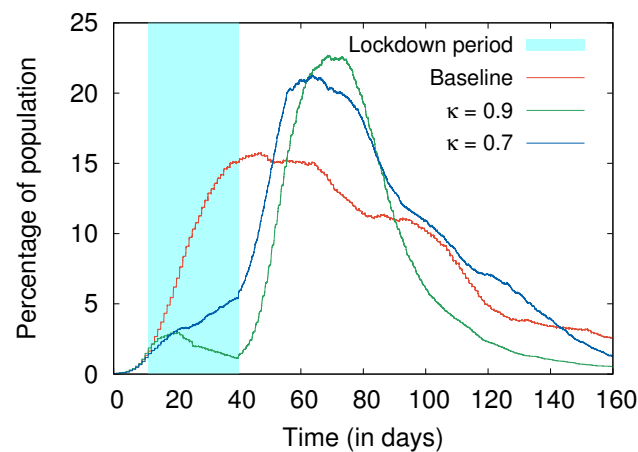


Figure 7. Effects of varying lockdown efficacy.

It also becomes apparent that once the lockdown is lifted, without any other policy, such as increased hygiene level or social distancing, we observe a worse peak than the baseline. This implies that a lockdown is not a complete solution, and can possibly only provide time to prepare for a later peak of infections. We can clearly see that lockdowns are effective at delaying the peak. Even with $\kappa = 0.7$, which means 30% of agents do not follow any guidelines, we do not see a high peak during the lockdown period.

If a partial lockdown is observed with (and followed by) higher social distancing and hygiene, there is some improvement. In Figure 8, we see that the proportion of infected agents stays at a moderately high level, but there is not a much higher peak, unlike in Figure 7.

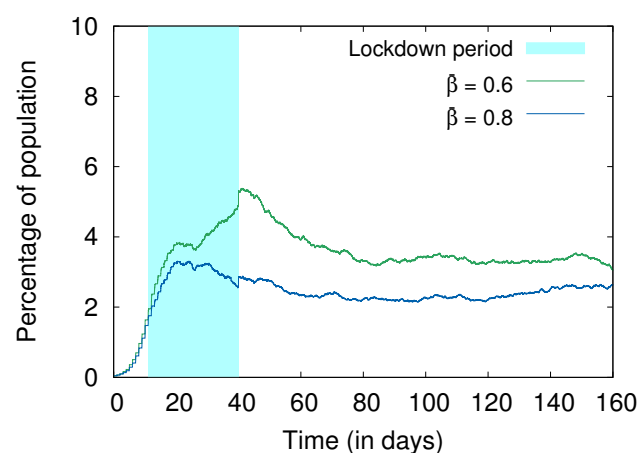


Figure 8. Effects of different levels of hygiene during and after lockdown with $\kappa = 0.8; \alpha = 0.7$.

We also present the the effect of social distancing post-lockdown. In Figure 9, we show the effects of varying levels of social distancing. Social distancing is a much more sensitive parameter compared to hygiene, so a small change in social distancing changes the number

of infections significantly. We can see that with a higher value of α (0.8), the proportion of infected agents is much lower than with a moderate value (0.6).

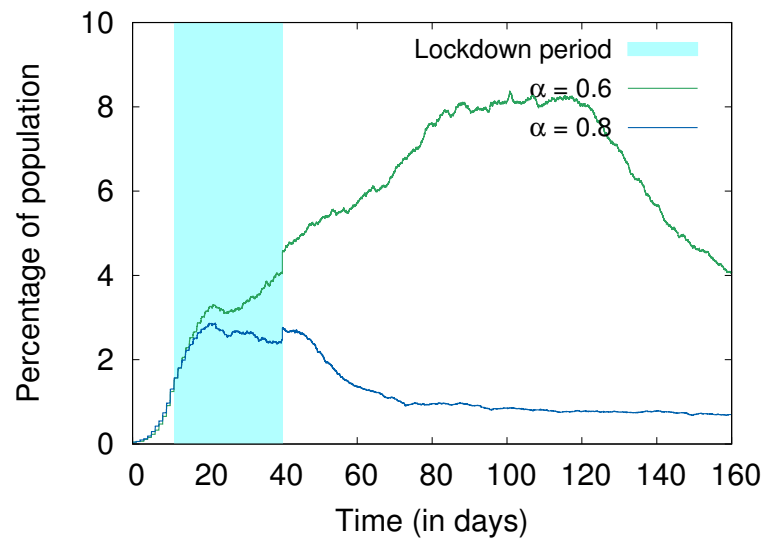


Figure 9. Effects of different levels of social distancing during and after lockdown with $\kappa = 0.8; \bar{\beta} = 0.6$.

4.5. Fractional Immunity

This set of experiments studies an initial state with some fraction of the population already immune to the virus (which can be achieved by natural immunity, post-infection recovery, or by vaccination). We describe this as fractional immunity in certain populations.

In one set of experiments, we started the simulation with baseline conditions (no hygiene or social distancing), but varying Π , the fractional immunity of the agent population, from 0.2 to 0.8 (corresponding to 20% through 80% of the population being immune). Figure 10 shows that even when 20% and 40% of population is immune to the virus, we can have significant peaks in infection in the absence of hygiene and social distancing. Even at 0.6 fractional immunity, there are a significant number of infections. It is only when there are 80% immune agents that we really see effective control of the spread of infection.

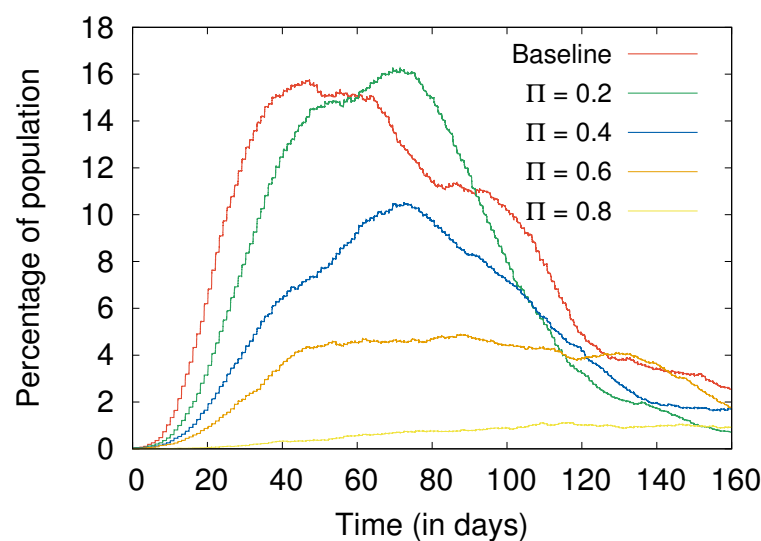
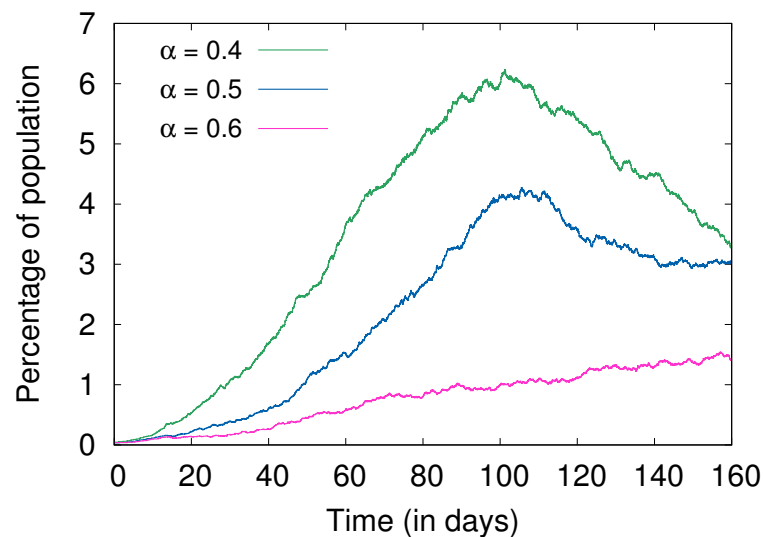


Figure 10. Effects of varying the levels of fractional immunity.

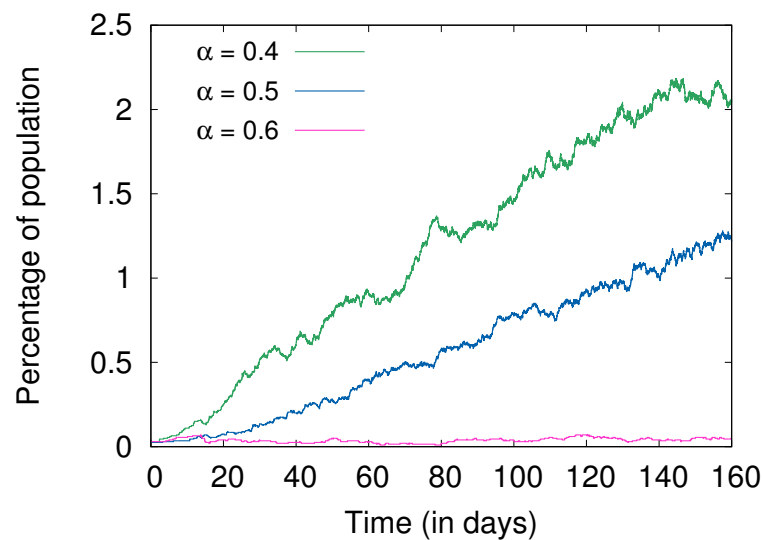
We experimented with varying levels of hygiene and social distancing with 20% and 40% of the population being immune.

Figure 11 shows the effect of varying social distancing, keeping $\bar{\beta}$ constant at 0.6, for Π at 0.2 and 0.4. As expected, the proportion of infected agents is lower with a higher value of Π (Figure 11a vs. Figure 11b). With a fractional immunity of 0.4 and moderate hygiene and social distancing, the value of the peak reached here is a fraction, roughly one-fourth, of the peak value seen for the same Π in Figure 10.

Similarly, Figure 12 shows the effects of varying hygiene with the social distancing efficacy kept constant at 0.6. We see a similar trend with the number of infections decreasing with increasing hygiene.

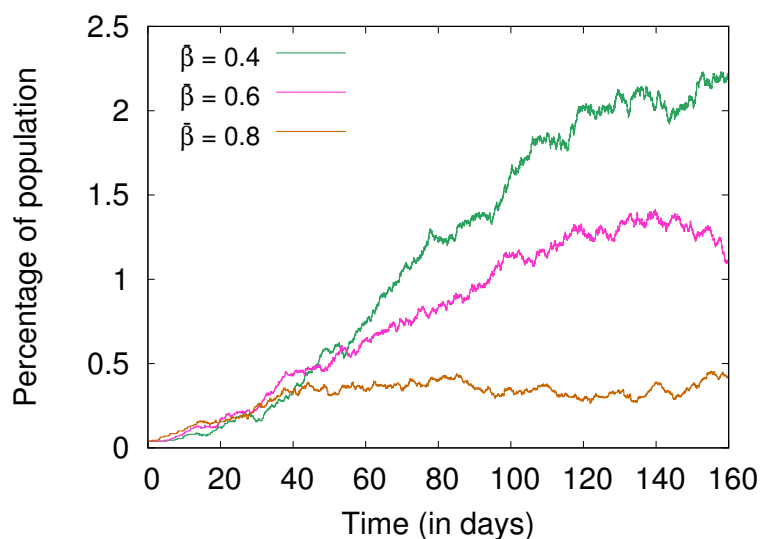


(a) $\Pi = 0.2, \bar{\beta} = 0.6$

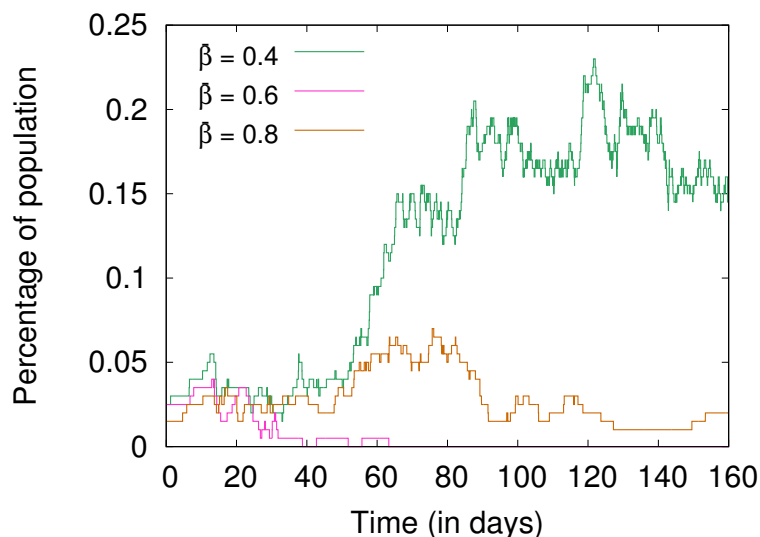


(b) $\Pi = 0.4, \bar{\beta} = 0.6$

Figure 11. Comparing the effects of α at two different levels of Π .



(a) $\Pi = 0.2, \alpha = 0.6$



(b) $\Pi = 0.4, \alpha = 0.6$

Figure 12. Comparing the effects of β at two different levels of Π .

4.6. Surges in Hospital Beds and ICUs

In this experiment, different levels of surge capacity were considered (50% increase, 100% increase in the bed capacity). On day 50, these surge capacities were added to the existing capacity. The purpose of this is to reduce the rate of death on account of inadequate hospital capacity.

Figure 13 shows the percentage of deceased agents. We can see that a surge reduces the number of deceased agents, but not in a linear fashion. The number of deceased agents drop by 10% by adding 50% more hospital and ICU beds, and further reduces by 20% when the number of beds and ICU units is doubled.

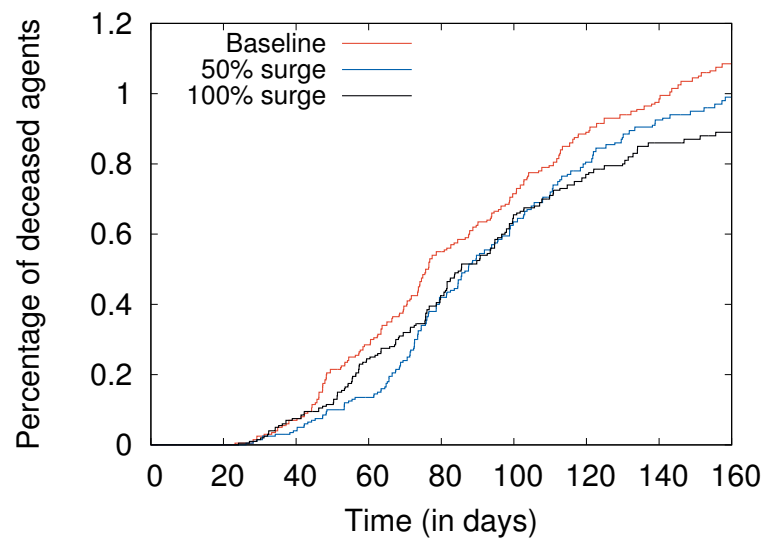


Figure 13. Common parameters across all three experiments ($\bar{\beta} = 0.6, \alpha = 0$): baseline ($b = 2$), 50% surge ($b = 3$), and 100% surge ($b = 4$).

5. Conclusions

Data-driven approaches and purely statistical models for COVID-19 exist, but have some significant limitations [53]. This is in large part due to the mostly unfamiliar nature of the novel coronavirus SARS-CoV-2, and the fact that traditional equation-based models fail to capture the dynamics of systems that are heavily dependent on factors such as population distributions and agent characteristics. Such top-down models are also ill-equipped to show the emergent consequences that arise from small changes in individual behaviors, and policy choices that cannot be readily expressed in mathematical form [16].

We, therefore, used an agent-based model for a qualitative assessment of the COVID-19 pandemic in an enclosed population where agents represent humans. This model is thus a bottom-up approach to capture the unpredictable interactions between members of a society, and understand the manner in which COVID-19 may spread under different conditions.

As COVID-19 is a new disease and its properties are still being discovered, it is possible that some assumptions of our model, which are in line with existing knowledge about the disease, may have to change. Nevertheless, we believe that this work demonstrates some important emergent properties and helps analyze what-if scenarios.

Even with a moderate level of personal hygiene and social distancing being widely observed, the epidemic can be effectively contained even with a relatively small fraction (such as 20–40%) of the population being immunized by vaccination or prior exposure and recovery. This means that dire prognostications that COVID-19 will eventually infect the majority of the population are fortunately unlikely.

Prior agent-based models for COVID-19, such as those by Silva et al. [18] and Cuevas [17], deal with a narrower set of possible circumstances. Our work is the first to provide conclusions about lockdowns and behavioral choices, such as personal hygiene and social distancing, and indicate the likely progress of the disease under specific conditions. It is our hope and expectation that this work will serve to illuminate certain aspects of the spread of the disease and show the value of certain types of control measures that may be applied. It should thus be of use to policy makers and authorities as well as the public at large.

Author Contributions: S.R. conceived the model and experiments, and A.T. implemented the code. A.T. and N.K.S. analyzed the results. A.T., N.K.S., and S.R. wrote and reviewed the manuscript. All authors have read and agreed to the published version of the manuscript.

Funding: This research received no external funding.

Institutional Review Board Statement: Not applicable.

Informed Consent Statement: Not applicable.

Data Availability Statement: The code and documentation for this work can be accessed from <https://github.com/ABM-for-Covid/ABM-for-Covid-19>. We have also created an interactive application <https://abmforcovid.org> for anyone to run experiments and tests with their own strategies.

Conflicts of Interest: The authors declare no conflict of interest.

References

1. Vynnycky, E.; White, R. *An Introduction to Infectious Disease Modelling*; Oxford University Press: Oxford, UK, 2010.
2. Keeling, M.J.; Rohani, P. *Modeling Infectious Diseases in Humans and Animals*; Princeton University Press: Princeton, NJ, USA, 2007.
3. Brauer, F.; Castillo-Chavez, C.; Feng, Z. *Mathematical Models in Epidemiology*; Texts in Applied Mathematics (Book 69); Springer: Berlin/Heidelberg, Germany, 2019.
4. Arino, J.; Brauer, F.; van den Driessche, P.; Watmough, J.; Wu, J. Simple models for containment of a pandemic. *J. R. Soc. Interface* **2006**, *3*, 453–457. [[CrossRef](#)]
5. Kim, S.; Lee, J.; Jung, E. Mathematical model of transmission dynamics and optimal control strategies for 2009 A/H1N1 influenza in the Republic of Korea. *J. Theor. Biol.* **2017**, *412*, 74–85. [[CrossRef](#)]
6. Arino, J.; Portet, S. A simple model of COVID-19. *Infect. Dis. Model.* **2020**, *5*, 309–315. [[CrossRef](#)]
7. Abdo, M.S.; Shah, K.; Wahash, H.A.; Panchal, S.K. On a comprehensive model of the novel coronavirus (COVID-19) under Mittag-Leffler derivative. *Chaos Solitons Fractals* **2020**, *135*, 109867. [[CrossRef](#)]
8. Gu, Y. COVID-19 Projections Using Machine Learning. Available online: <https://covid19-projections.com/> (accessed on 16 October 2020).
9. New America. *Pandemic Response Repository*; New America: New York, NY, USA, 2020.
10. Perez, L.; Dragicevic, S. An agent-based approach for modeling dynamics of contagious disease spread. *Int. J. Health Geogr.* **2009**, *8*, 50. [[CrossRef](#)] [[PubMed](#)]
11. Miksch, F.; Urach, C.; Einzinger, P.; Zauner, G. A Flexible Agent-Based Framework for Infectious Disease Modeling. In *Information and Communication Technology–EurAsia Conference (ICT-EurAsia 2014)*; Linawati, Mahendra, M.S., Neuhold, E.J., Tjoa, A.M., You, I., Eds.; Springer: Berlin/Heidelberg, Germany, 2014; pp. 36–45. [[CrossRef](#)]
12. Hunter, E.; Mac Namee, B.; Kelleher, J. An open-data-driven agent-based model to simulate infectious disease outbreaks. *PLoS ONE* **2018**, *13*, e0208775. [[CrossRef](#)] [[PubMed](#)]
13. Tracy, M.; Cerdá, M.; Keyes, K.M. Agent-Based Modeling in Public Health: Current Applications and Future Directions. *Annu. Rev. Public Health* **2018**, *39*, 77–94. [[CrossRef](#)]
14. Jindal, A.; Rao, S. Agent-Based Modeling and Simulation of Mosquito-Borne Disease Transmission. In *Proceedings of the Sixteenth International Conference on Autonomous Agents and Multiagent Systems (AAMAS 2017)*, São Paulo, Brazil, 8–12 May 2017; pp. 426–435.
15. Khalil, K.M.; Abdel-Aziz, M.; Nazmy, T.T.; Salem, A.B.M. An agent-based modeling for pandemic influenza in Egypt. In *Proceedings of the 7th International Conference on Informatics and Systems (INFOS 2010)*, Cairo, Egypt, 28–30 March 2010; [[CrossRef](#)]
16. Hunter, E.; Mac Namee, B.; Kelleher, J. A Comparison of Agent-Based Models and Equation Based Models for Infectious Disease Epidemiology. In *Proceedings of the 26th AIAI Irish Conference on Artificial Intelligence and Cognitive Science (AICS 2018)*, Dublin, Ireland, 6–7 December 2018; pp. 33–44. Available online: http://ceur-ws.org/Vol-2259/aics_5.pdf (accessed on 16 October 2020).
17. Cuevas, E. An agent-based model to evaluate the COVID-19 transmission risks in facilities. *Comput. Biol. Med.* **2020**, *121*, 103827. [[CrossRef](#)]
18. Silva, P.C.L.; Batista, P.V.C.; Lima, H.S.; Alves, M.A.; Guimarães, F.G.; Silva, R.C.P. COVID-ABS: An Agent-Based Model of COVID-19 Epidemic to Simulate Health and Economic Effects of Social Distancing Interventions. *Chaos Solitons Fractals* **2020**, *139*, 110088. [[CrossRef](#)] [[PubMed](#)]
19. del Rio, C.; Malani, P.N. COVID-19—New Insights on a Rapidly Changing Epidemic. *JAMA* **2020**, *323*, 1339–1340. [[CrossRef](#)]
20. Arabi, Y.M.; Murthy, S.; Webb, S. COVID-19: A novel coronavirus and a novel challenge for critical care. *Intensive Care Med.* **2020**, *46*, 833–836; Corrected in *Intensive Care Med.* **2020**, *46*, 1087–1088. [[CrossRef](#)]
21. Schueller, E.; Klein, E.; Tseng, K.; Kapoor, G.; Joshi, J.; Sriram, A.; Nandi, A.; Laxminarayan, R. *COVID-19 in India: Potential Impact of the Lockdown and Other Longer-Term Policies*; Center for Disease Dynamics, Economics & Policy (CDDEP): Washington, DC, USA, 2020.
22. Randolph, H.E.; Barreiro, L.B. Herd Immunity: Understanding COVID-19. *Immunity* **2020**, *52*, 737–741. [[CrossRef](#)]
23. Sun, C.; Hsieh, Y.H. Global analysis of an SEIR model with varying population size and vaccination. *Appl. Math. Model.* **2010**, *34*, 2685–2697. [[CrossRef](#)]
24. Feng, Z. Final and peak epidemic sizes for SEIR models with quarantine and isolation. *Math. Biosci. Eng.* **2007**, *4*, 675–686. [[CrossRef](#)] [[PubMed](#)]

25. Bai, Y.; Yao, L.; Wei, T.; Tian, F.; Jin, D.Y.; Chen, L.; Wang, M. Presumed Asymptomatic Carrier Transmission of COVID-19. *JAMA* **2020**, *323*, 1406–1407. [[CrossRef](#)]
26. Last, J.M. (Ed.) *A Dictionary of Public Health*; Oxford University Press: Oxford, UK, 2007.
27. Erren, T.C. Shift work, cancer and “white-box” epidemiology: Association and causation. *Epidemiol. Perspect. Innov.* **2010**, *7*, 11. [[CrossRef](#)] [[PubMed](#)]
28. van den Driessche, P. Reproduction numbers of infectious disease models. *Infect. Dis. Model.* **2017**, *2*, 288–303. [[CrossRef](#)]
29. Delamater, P.L.; Street, E.J.; Leslie, T.F.; Yang, Y.T.; Jacobsen, K.H. Complexity of the Basic Reproduction Number (R_0). *Emerg. Infect. Dis.* **2019**, *25*, 1–4. [[CrossRef](#)] [[PubMed](#)]
30. Li, J.; Blakeley, D.; Smith, R.J. The Failure of R_0 . *Comput. Math. Model. Med.* **2011**, *2011*, 527610. [[CrossRef](#)]
31. Davies, N.G.; Klepac, P.; Liu, Y.; Prem, K.; Jit, M.; CMMID COVID-19 Working Group; Eggo, R.M. Age-dependent effects in the transmission and control of COVID-19 epidemics. *Nat. Med.* **2020**, *26*, 1205–1211. [[CrossRef](#)] [[PubMed](#)]
32. Sanyaolu, A.; Okorie, C.; Marinkovic, A.; Patidar, R.; Younis, K.; Desai, P.; Hosein, Z.; Padda, I.; Mangat, J.; Altaf, M. Comorbidity and its Impact on Patients with COVID-19. *SN Compr. Clin. Med.* **2020**, *2*, 1069–1076. [[CrossRef](#)]
33. Hermesh, T.; Moltedo, B.; López, C.B.; Moran, T.M. Buying time—The immune system determinants of the incubation period to respiratory viruses. *Viruses* **2010**, *2*, 2541–2558. [[CrossRef](#)] [[PubMed](#)]
34. Gardner, I.D. The Effect of Aging on Susceptibility to Infection. *Rev. Infect. Dis.* **1980**, *2*, 801–810. [[CrossRef](#)]
35. Ashby, B.; Bruns, E. The evolution of juvenile susceptibility to infectious disease. *Proc. R. Soc. B* **2018**, *285*, 20180844. [[CrossRef](#)] [[PubMed](#)]
36. Prakash, B.; Adamic, L.; Iwashyna, T.; Tong, H.; Faloutsos, C. Fractional immunization in networks. In Proceedings of the SIAM International Conference on Data Mining 2013 (SMD 2013), Austin, TX, USA, 2–4 May 2013; Society for Industrial and Applied Mathematics Publications: Philadelphia, PA, USA, 2013; pp. 659–667. [[CrossRef](#)]
37. Hanley, B. An object simulation model for modeling hypothetical disease epidemics—EpiFlex. *Theor. Biol. Med. Model.* **2006**, *3*, 32. [[CrossRef](#)] [[PubMed](#)]
38. Kirkeby, C.; Halasa, T.; Gussmann, M.; Toft, N.; Græsbøll, K. Methods for estimating disease transmission rates: Evaluating the precision of Poisson regression and two novel methods. *Sci. Rep.* **2017**, *7*, 9496. [[CrossRef](#)]
39. Stehlé, J.; Voirin, N.; Barrat, A.; Cattuto, C.; Colizza, V.; Isella, L.; Régis, C.; Pinton, J.F.; Khanafer, N.; den Broeck, W.V.; et al. Simulation of an SEIR infectious disease model on the dynamic contact network of conference attendees. *BMC Med.* **2011**, *9*, 87. [[CrossRef](#)]
40. Liu, Y.; Gayle, A.A.; Wilder-Smith, A.; Rocklöv, J. The reproductive number of COVID-19 is higher compared to SARS coronavirus. *J. Travel Med.* **2020**. [[CrossRef](#)]
41. Virlogeux, V.; Fang, V.J.; Wu, J.T.; Ho, L.M.; Peiris, J.S.M.; Leung, G.M.; Cowling, B.J. Brief Report: Incubation Period Duration and Severity of Clinical Disease Following Severe Acute Respiratory Syndrome Coronavirus Infection. *Epidemiology* **2015**, *26*, 666. [[CrossRef](#)]
42. CDC. Symptoms of Coronavirus. 2020. Available online: <https://www.cdc.gov/coronavirus/2019-ncov/symptoms-testing/symptoms.html> (accessed on 16 October 2020).
43. Li, Q.; Guan, X.; Wu, P.; Wang, X.; Zhou, L.; Tong, Y.; Ren, R.; Leung, K.S.; Lau, E.H.; Wong, J.Y.; et al. Early Transmission Dynamics in Wuhan, China, of Novel Coronavirus-Infected Pneumonia. *N. Engl. J. Med.* **2020**, *382*, 1199–1207. [[CrossRef](#)]
44. Sakurai, A.; Sasaki, T.; Kato, S.; Hayashi, M.; Tsuzuki, S.I.; Ishihara, T.; Iwata, M.; Morise, Z.; Doi, Y. Natural History of Asymptomatic SARS-CoV-2 Infection. *N. Engl. J. Med.* **2020**, *383*, 885–886. [[CrossRef](#)]
45. CDC. Duration of Isolation and Precautions for Adults with COVID-19. 2020. Available online: <https://www.cdc.gov/coronavirus/2019-ncov/hcp/duration-isolation.html> (accessed on 16 October 2020).
46. Marfil-Garza, B.A.; Belaunzarán-Zamudio, P.F.; Guliás-Herrero, A.; Zuñiga, A.C.; Caro-Vega, Y.; Kershenobich-Stalnikowitz, D.; Sifuentes-Osornio, J. Risk factors associated with prolonged hospital length-of-stay: 18-year retrospective study of hospitalizations in a tertiary healthcare center in Mexico. *PLoS ONE* **2018**, *13*, e0207203. [[CrossRef](#)] [[PubMed](#)]
47. WHO. European Health Information Gateway. 2020. Available online: https://gateway.euro.who.int/en/indicators/hfa_478-5060-acute-care-hospital-beds-per-100-000/ (accessed on 16 October 2020)
48. Johansson, A.; Helbing, D.; Al-Abideen, H.Z.; Al-Bosta, S. From crowd dynamics to crowd safety: A video-based analysis. *Adv. Complex Syst.* **2008**, *11*, 497–527. [[CrossRef](#)]
49. Romanczuk, P.; Couzin, I.D.; Schimansky-Geier, L. Collective motion due to individual escape and pursuit response. *Phys. Rev. Lett.* **2009**, *102*, 010602. [[CrossRef](#)]
50. Luke, S.; Cioffi-Revilla, C.; Panait, L.; Sullivan, K.; Balan, G. MASON: A Multiagent Simulation Environment. *Simulation* **2005**, *81*, 517–527. [[CrossRef](#)]
51. Harpaz, R.; Dahl, R.M.; Dooling, K.L. Prevalence of Immunosuppression Among US Adults, 2013. *JAMA* **2016**, *316*, 2547–2548. [[CrossRef](#)]
52. Poletti, P.; Tirani, M.; Cereda, D.; Trentini, F.; Guzzetta, G.; Sabatino, G.; Marziano, V.; Castrofino, A.; Grosso, F.; Del Castillo, G.; et al. Probability of symptoms and critical disease after SARS-CoV-2 infection. *arXiv* **2020**, arXiv:2006.08471.
53. Siegenfeld, A.F.; Taleb, N.N.; Bar-Yam, Y. Opinion: What models can and cannot tell us about COVID-19. *Proc. Natl. Acad. Sci. USA* **2020**, *117*, 16092–16095. [[CrossRef](#)]